Michigan Technological University

Digital Commons @ Michigan Tech

Department of Geological and Mining Engineering and Sciences Publications

Department of Geological and Mining Engineering and Sciences

2-1-1999

Early evolution of a stratospheric volcanic eruption cloud as observed with TOMS and AVHRR

David J. Schneider
Michigan Technological University

William I. Rose
Michigan Technological University

Larry R. Coke
Michigan Technological University

Gregg J. Bluth
Michigan Technological University

Ian E. Sprod
NASA Goddard Space Flight Center

See next page for additional authors

Follow this and additional works at: https://digitalcommons.mtu.edu/geo-fp

Part of the Geology Commons, Mining Engineering Commons, and the Other Engineering Commons

Recommended Citation

Schneider, D. J., Rose, W. I., Coke, L. R., Bluth, G. J., Sprod, I. E., & Krueger, A. J. (1999). Early evolution of a stratospheric volcanic eruption cloud as observed with TOMS and AVHRR. *Geophysical Research Letters, 104*(D4), 4037-4050. http://dx.doi.org/10.1029/1998JD200073
Retrieved from: https://digitalcommons.mtu.edu/geo-fp/82

Follow this and additional works at: https://digitalcommons.mtu.edu/geo-fp

Part of the Geology Commons, Mining Engineering Commons, and the Other Engineering Commons

Authors

David J. Schneider, William I. Rose, Larry R. Coke, Gregg J. Bluth, Ian E. Sprod, and Arlin J. Krueger

This article is available at Digital Commons @ Michigan Tech: https://digitalcommons.mtu.edu/geo-fp/82

JOURNAL OF GEOPHYSICAL RESEARCH, VOL. 104, NO. D4, PAGES 4037-4050, FEBRUARY 27, 1999

Early evolution of a stratospheric volcanic eruption cloud as observed with TOMS and AVHRR

David J. Schneider[1], William I. Rose, Larry R. Coke, and Gregg J.S. Bluth
Department of Geological Engineering and Sciences, Michigan Technological University, Houghton

Ian E. Sprod[2] and Arlin J. Krueger
NASA Goddard Space Flight Center, Greenbelt, Maryland

Abstract. This paper is a detailed study of remote sensing data from the total ozone mapping spectrometer (TOMS) and the advanced very high resolution radiometer (AVHRR) satellite detectors, of the 1982 eruption of El Chichón, Mexico. The volcanic cloud/atmosphere interactions in the first four days of this eruption were investigated by combining ultraviolet retrievals to estimate the mass of sulfur dioxide in the volcanic cloud [*Krueger et al.*, 1995] with thermal infrared retrievals of the size, optical depth, and mass of fine-grained (1- 10 μm radius) volcanic ash [*Wen and Rose*, 1994]. Our study provides the first direct evidence of gravitational separation of ash from a stratospheric, gas-rich, plinian eruption column and documents the marked differences in residence times of volcanic ash and sulfur dioxide in volcanic clouds. The eruption column reached as high as 32 km [*Carey and Sigurdsson*, 1986] and was injected into an atmosphere with a strong wind shear, which allowed for an observation of the separation of sulfur dioxide and volcanic ash. The upper, more sulfur dioxide-rich part of the cloud was transported to the west in the stratosphere, while the fine-grained ash traveled to the south in the troposphere. The mass of sulfur dioxide released was estimated at 7.1 x 10^9 kg with the mass decreasing by approximately 4% 1 day after the peak. The mass of fine-grained volcanic ash detected was estimated at 6.5 x 10^9 kg, amounting to about 0.7% of the estimated mass of the ash which fell out in the mapped ash blanket close to the volcano. Over the following days, 98% of this remaining fine ash was removed from the volcanic cloud, and the effective radius of ash in the volcanic cloud decreased from about 8 μm to about 4 μm.

1. Introduction

Satellite sensors are now the only consistently available tools to synoptically and comprehensively measure volcanic eruption clouds, which are an important natural hazard to aircraft [*Casadevall,* 1994] and which host important chemical reactions, leading to the formation of atmospheric sulfate aerosols [*Self et al.,* 1981; *Rose and Chesner,* 1987; *Pinto et al.,* 1989; *Tabazadeh and Turco,* 1993]. Data from the total ozone mapping spectrometer (TOMS) are used to calculate the mass of SO_2 in volcanic clouds for several days to weeks after eruption [*Krueger et al.,* 1995], while the advanced very high resolution radiometer (AVHRR) and GOES- 8 and GOES- 9 can detect and measure the sizes and masses of ash particles in volcanic clouds for similar, although shorter periods [*Wen and Rose,* 1994; *Schneider et al.,* 1995; *Rose and Schneider,* 1996]. Although data from both TOMS and AVHRR have been available since about 1981, to date most studies have focused on only one sensor. However, combined use of these sensors allows for evaluation of some possible reactions in volcanic clouds [*Rose et al.,* 1995]. In this paper we present a comprehensive application of comparative TOMS and AVHRR data by applying them to the 1982 eruption of El Chichón, Mexico, one of two eruptions in the past 20 years with atmospheric aerosol loading estimated at greater than 10 Tg [*McCormick et al.,* 1994].

Comparison of 10 AVHRR images and five TOMS images are presented in this paper (Table 1). They document the injection, movement, and removal of SO_2 and fine-grained (1-10 μm radius) volcanic ash from April 4 to April 7, 1982. This comparison clearly demonstrates that within the first day after eruption El Chichón's volcanic cloud separated into two: one stratospheric cloud contained SO_2 and very little volcanic ash, while the second had little SO_2, with comparatively large masses of ash, and resided in the troposphere. Although the TOMS instrument has provided a systematic measurement of the emission of SO_2 since 1979, there have not been similar measurements of the amount of volcanic ash released by explosive eruptions. This paper contains the first systematic application of the volcanic cloud retrieval algorithm of *Wen and Rose* [1994] to a time series of AVHRR satellite data. Height estimates of the clouds are made by comparing cloud movement to a trajectory model developed by *Schoeberl et al.* [1992] (Figure 1). A gravitational settling model is proposed, and ash particle settling calculations are presented. The significance of the separation of ash and SO_2 to atmospheric processes and volcanic hazards is discussed.

Three major explosive eruptions of El Chichón (17.33° N; 93.20°W) occurred on March 29, 1982 at 0532 UT, April 4, 1982 at 0135 UT, and April 4, 1982 at 1122 UT and have been designated on the basis of tephra fall deposits as the A-1, B, and C eruptions, respectively [*Sigurdsson et al.,* 1984; *Varekamp et al.,* 1984] (Table 2). These events together were observed and mapped using

[1]Now at Raytheon STX, U. S. Geological Survey, Alaska Volcano Observatory, Anchorage.

[2]Now at Cooperative Institute for Research in Environmental Sciences, Boulder, Colorado.

Copyright 1999 by the American Geophysical Union.

Paper number 1998JD200073.
0148-0227/99/1998JD200073$09.00

Table 1. List of 1982 Satellite Data Used in This Study.

Date	Time, UT	Detected	Sensor	Plate
April 4	0805 and 0945	Ash	AVHRR	1a
April 4	1820	SO_2	TOMS	1b
April 4	2100	Ash	AVHRR	1c
April 5	0755 and 0930	Ash	AVHRR	1d
April 5	1700 and 1840	SO_2	TOMS	1e
April 5	2045 and 2230	Ash	AVHRR	1f
April 6	1720 and 1900	SO_2	TOMS	1g
April 6	2035 and 2215	Ash	AVHRR	1h
April 7	0915 and 1050	Ash	AVHRR	1i

geostationary satellite data [*Matson,* 1984], and the stratospheric cloud was tracked for 3 weeks using both visible and thermal infrared bands of the GOES-E, GOES-W, and NOAA 7 satellites [*Robock and Matson,* 1983]. The B and C eruptions together injected an estimated 7.0 (± 2.1) x 10^9 kg of SO_2 [*Bluth et al.,* 1992] into the atmosphere and produced an estimated global temperature decrease of about 0.2°C [*Pinto et al.,* 1989].

Mapping of the tephra fall deposits showed that the heaviest deposition from the B and C events occurred ENE of the vent [*Sigurdsson et al.*, 1984; *Varekamp et al.*, 1984], and normal grading in the deposits indicate that the maximum column height occurred at the start of each event, and then decreased with time [*Carey and Sigurdsson,* 1986].

2. Detection and Measurement of Volcanic Ash Using AVHRR

Thermal image data from two channels of the AVHRR were used in this study. Band 4 (10.3 to 11.3 µm) minus band 5 (11.5 to 12.5 µm) brightness temperature differences (BTD) are used to detect the volcanic cloud and distinguish it from meteorological clouds. Semitransparent volcanic clouds are known to have negative band 4 minus 5 BTD [*Prata,* 1989; *Wen and Rose,* 1994; *Schneider et al.,* 1995], while meteorological clouds generally have positive BTD [*Yamanouchi et al.,* 1987]. The cloud optical depth and the size and mass of particles in the clouds were retrieved using the technique of *Wen and Rose* [1994], and the results are shown in Plate 1 and Table 3. The retrievals are model-dependent and assume a single-layer, partially transparent cloud, composed entirely of spherical andesite ash particles having a log-normal size distribution, which is parallel to a homogeneous underlying surface, with a clear atmosphere above the cloud as well as between the cloud and the surface beneath it. The limitations of results obtained for volcanic clouds using these assumptions are discussed in a later section.

3. Detection and Measurement of Sulfur Dioxide Using TOMS

The sulfur dioxide index was calculated by the technique outlined by *Krueger et al.* [1995], and is shown in Plate 1. TOMS measures the Earth's ultraviolet (UV) albedo, which is the ratio of backscattered Earth radiance to incoming solar irradiance, in six bands centered at 312.5, 317.5, 331.2, 339.8, 360.0, and 380.0 nm. The total column abundance of SO_2 is determined by its characteristic attenuation of the UV albedo in the four shortest TOMS bands. The tonnage of SO_2 over a given region is obtained by multiplying the column amounts by their ground surface areas, which vary from 2500 km^2 at the nadir to 19,000 km^2 at the edge of the swath. Empirical corrections are used to offset the linear effects that variations in ozone, surface reflectance, and scan bias can impart on the SO_2 calculations. Sulfur dioxide concentrations are presented in Dobson units (DU), which are equivalent to milliat-

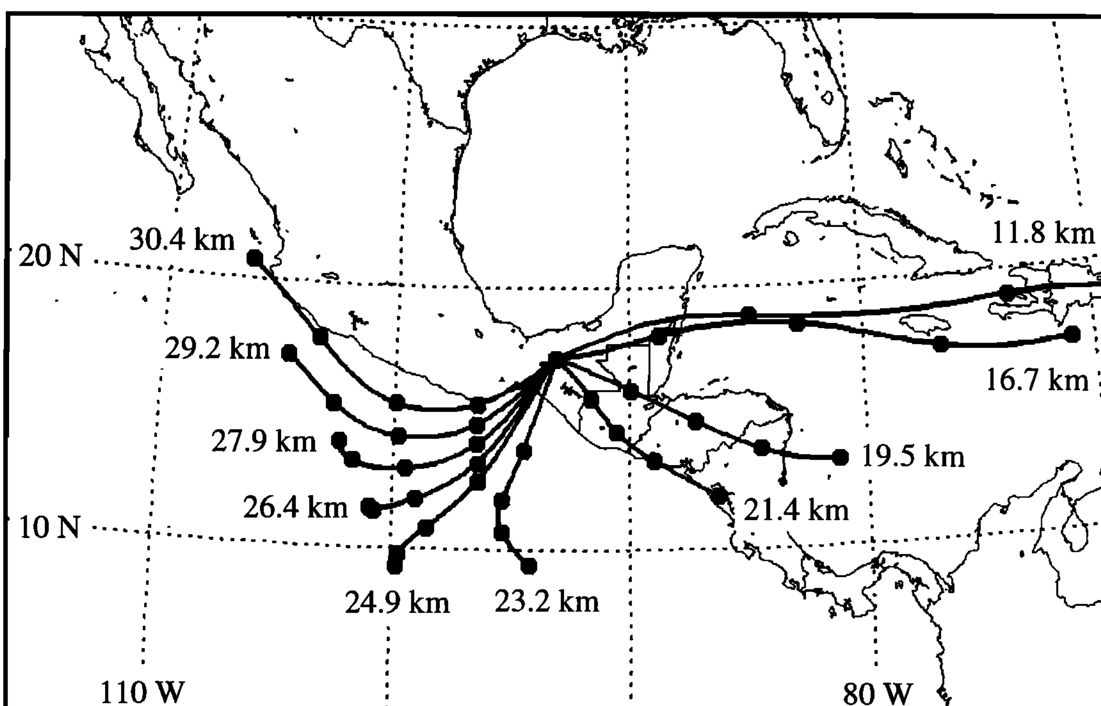

Figure 1. Trajectory plot of air parcels from 11.8 to 30.4 km altitude, from the model of *Schoeberl et al.* [1992]. The trajectories start at the volcano at 1200 UT on April 4, 1982, and continue for 48 hours, with dots along each trajectory path corresponding to a 12 hour time increment.

Table 2. Chronology of 1982 Eruptions of El Chichón.

Start Time, UT	Fall Unit	Duration, h	Fallout Mass, kg	Column Height, km
March 29, 0532	A-1	6	2.6×10^{11}	20 to 27
April 4, 0135	B	4.5	4.9×10^{11}	24 to 32
April 4, 1122	C	7	4.2×10^{11}	22 to 29

Sigurdsson et al., [1984]; *Varekamp et al.*, [1984]; *Carey and Sigurdsson* [1986].

mosphere centimeters, the column thickness of the gas at standard temperature and pressure. Mass estimates are reported with an estimated error of ±30%. There are currently two different algorithms that are used in TOMS SO_2 retrievals, called version 6 [*Krueger et al.*,1995] and version 7 respectively. Version 7 has some inherent improvements because it also measures an "aerosol index" which shows the distribution of silicate ash, but does not fully quantify it [*Seftor et al.*, 1997; *Krotkov et al.*, 1997]. In this study we used version 6 only because as of this writing version 7 is still being refined for volcanic cloud study. For example, version 7 cannot in its current state measure pixels with >205 DU [*McPeters et al.*, 1996], and these are abundant in the El Chichón clouds.

4. Cloud Height and Trajectory Estimates

In the tropics north of the equator in the spring winds are typically westerly in the troposphere and easterly in the stratosphere. Because it seemed that the detected volcanic clouds would reflect differences in winds at different levels, we needed to verify this condition, at least qualitatively. Although 1982 National Meteorological Center (NMC) wind field data is rather poor for the tropics, we nonetheless applied the trajectory model described by *Schoeberl et al.* [1992]. In this model, parcels are advected by winds derived from the NMC's balanced wind equation and interpolated to isentropic (constant potential temperature) surfaces. The winds at a given time are interpolated from the previous and subsequent data sets, which are available every 12 hours (0000 and 1200 UT). The range of potential temperature surfaces, corresponding to altitudes from about 12 to 30 km, is shown in Figure 1. The altitudes plotted in the diagram are only approximate (± 1-2 km) because the height range estimates change with time and location. Here we use them only to show what the atmosphere motion may have been.

The trajectories start at the volcano at 1200 UT on April 4, 1982, and continue for 48 hours, with dots along each trajectory corresponding to a 12 hour time increment. Although they contain large errors which are hard to quantify, the trajectory analysis shows NE to easterly winds at altitudes of about 23-30 km, northerly to NW winds at about 19-23 km, and westerly winds at about 12-19 km altitudes. This highly approximate pattern of wind shear is generally consistent with the observed movement of clouds as shown in Plate 1, with the tropopause at about 17-18 km. In spite of the poor NMC data and uncertainty in the actual heights, we think it is unlikely that the relative positions of the wind vectors are incorrect.

5. TOMS and AVHRR Observations

The first AVHRR images of the volcanic ash cloud from the B eruption are shown in Plate 1a as a composite of images collected at 0805 and 0945 UT (0205 and 0345 local time), approximately 6.5 to 8 hours after the start, and 2.5 to 4 hours after the end of the B event. Although several previous researchers [e.g., *Matson*, 1984] have shown that the volcanic ash cloud dispersed in two main directions, east-northeast (ENE) and west-southwest (WSW), the AVHRR retrievals show that the main mass of fine-grained (1-10 μm radius) silicate ash was transported ENE of the vent, with lesser amounts moving WSW. The region of the cloud with the highest retrieved mass correlates to the area with the thickest tephra fallout on the ground: however, this is coincidental, reflecting the rapid fallout (within 4-8 hours from the onset of B) of the bulk of the El Chichón ash toward the ENE. AVHRR detects ash which is fine-grained, and therefore did not fall out quickly to become incorporated in the tephra deposits, and the image (Plate 1a) maps fine ash (1-10 μm in radius) which was still at elevated altitude. The mass of fine ash in an opaque region of the cloud (extending eastward from the vent to the Guatemala border) could not be determined due to its high optical depth, but this is likely the region with the greatest mass. The mass retrieved (Table 3) is therefore a minimum that greatly underestimates the true ash volumes (see also section 7). The trajectory analysis (Figure 1) suggests that the altitude of the ENE portion of the cloud was between 16 and 20 km and that the WSW portion of the volcanic cloud was most likely higher than 25 km.

The first TOMS image of the sulfur dioxide cloud (Plate 1b) was collected on April 4 at 1820 UT (1220 local time), near the end of the C eruption. This image shows the bidirectional spreading of the SO_2. Unlike the ash dispersal mapped by AVHRR, the highest concentration of SO_2 extends to the west of the vent, with lesser amounts extending to the east. Assuming that the SO_2 at the leading edges of the cloud was emitted at the start of the B event, the velocity of the western edge of the SO_2 cloud is approximately 12 m/s, and the velocity of the eastern edge is about 25 m/s. The maximum height of the SO_2 cloud likely extends from approximately 14-16 km in the ENE direction to greater than 25 km in the WSW direction.

The volcanic ash cloud mapped from AVHRR data collected on April 4 at 2100 UT (about 2.5 hours after the end of the C eruption) shows that the main mass of ash from the B and C eruptions extends to the east of the vent, with lesser amounts extending toward the west (Plate 1c). Ash from the B eruption (which had ended 15 hours earlier) had separated into two clouds. The main mass of ash from the B event is observed over Honduras, Guatemala, and the Gulf of Mexico, following a trajectory with is consistent with an altitude of approximately 18-20 km (Figure 1). The velocity of the western edge of the cloud is 12 m/s, which is identical to the velocity of the western edge of the SO_2 cloud shown in Plate 1b. The main mass of ash from the C eruption extends east of the vent, with a subsidiary mass extending to the west (Plate 1c). Note that the mass of a significant portion of the cloud, over the Yucatan Peninsula (red dotted outline) could not be determined in this image due to its high optical depth, and that presumably this is the region with the greatest silicate mass. The trajectory analysis (Figure 1) suggests that the altitude of the ENE portion of the cloud was between 16 and 20 km and that the WSW portion of the volcanic cloud was most likely higher than 25 km.

By the time of the next AVHRR scene (April 5 at 0755 and 0930 UT), the entire volcanic cloud had become partially transparent, allowing for a mass retrieval of the whole cloud (Plate 1d). Two ash clouds are seen in this image: a small cloud over the Pacific Ocean (centered at 18°N and 107°W), and the main cloud extending for 2500 km from 80°W to 100°W and from 12°N to 21°N. Although it was not easily identified in the previous

AVHRR image (Plate 1c), the small cloud over the Pacific Ocean is likely from the start of the B eruption. Analysis of the tephra fall deposits by *Carey and Sigurdsson* [1986] indicated that the maximum cloud height of the B and C eruptions was at the start of the event, and that the cloud height decreased with time. Thus it is likely that the small cloud from over the Pacific Ocean is ash from the start of the B eruption, and that it is likely higher than the main cloud over Central America. The main mass of ash (located over Guatemala and Belize) moved SE of the vent at an altitude of approximately 19-21 km. Shearing of the top and bottom of the cloud transported ash to the SW in the stratosphere and to the NE in the troposphere.

Separation of the ash and sulfur dioxide is more pronounced in subsequent images. Plate 1e is a composite map of two successive TOMS swaths collected at 1700 and 1840 UT on April 5. Three discrete regions of high SO_2 values can be observed in this image. Region 1, the most westerly edge of the plume, is 2200 km from the vent and extends from 14°N to 20°N and from 114°W to 105°W. If this region of SO_2 was emitted at the start of eruption B, the velocity of the leading edge would be about 15 m/s. Comparisons between the rate of cloud movement and radiosonde wind data indicate that the altitude of this portion of the cloud is approximately 26-28 km, which is consistent with lidar measurements from the Mauna Loa Observatory, Hawaii, taken on April 9, 1982 [*DeLuisi et al.*, 1983], with airborne and ground-based lidar measurements of stratospheric aerosol from June 1982 until January 1984 [*McCormick et al.*, 1984], and with balloon-borne sampling from May to December 1982 [*Hofmann and Rosen*, 1983]. Another high SO_2 concentration in Plate 1e is centered at 18°N and 98°W, and is designated region 2. Its leading (westward) edge is difficult to define, but the center of the cloud is located about 500 km west of the vent. A third area of high SO_2 extends 200 km west of the volcano, and is designated region 3. Lower values of SO_2 extend to the east from the vent, probably reflecting SO_2 moving in the troposphere from both the B and C eruptions.

Plate 1f is a composite map from AVHRR data collected at 2045 and 2230 UT on April 5. By this time the patterns shown by the two detectors differ sharply. An area of volcanic ash from the start of the B eruption is detected at 14°N to 22°N, 116°W to 105°W, in the same area as the most westerly SO_2 concentration in Plate 2e. This indicates that some of the SO_2 and ash from the B event traveled together for at least 45 hours. The main mass of volcanic ash from the C event is centered over southern Guatemala, Honduras, and El Salvador, with a "tail" extending to the west. The trajectory of this portion of the cloud indicates an altitude of 19-21 km (Figure 1). Shearing of the bottom of the cloud by westerly tropospheric winds has greatly diminished from the previous image (Plate 1d), and the fallout of coarser ash has likely occurred, so that the residual ash cloud is virtually neutrally buoyant. The top of the cloud continues to be sheared by strong easterly stratospheric winds, resulting in the production of the "tail". A third area of ash is detected near the vent, possibly due to additional eruptive activity following the C event.

By April 6 (Plate 1g and 1h), the SO_2 and ash clouds continue to move in different directions. In general, the main mass of SO_2 moved to the west, and the main mass of ash moved toward the south. The western edge of the SO_2 cloud (region 1) had moved to the west beyond the field of the image at a rate of 15 m/s. The center of the SO_2 mass designated as region 2 moved to the northwest from its location on April 5 at a rate of 9 m/s, and developed a plume structure extending southwest for more than 700 km. The center of the SO_2 mass designated as region 3 moved slowly (2 m/s) to the northeast from its location on April 5 and developed a plume extending to the southwest for more than 1300 km. The development of the plume structures is likely due to shear at the top of the SO_2 clouds by strong northeasterly winds (10-20 m/s) at altitudes from 23.8 to 26.5 km (radiosonde wind data from Veracruz, Mexico on April 5 and 6). Lower concentrations of SO_2 extend to the east, reflecting SO_2 carried in the troposphere. The volcanic ash from the C eruption continued to move to the south

Plate 1. The El Chichón volcanic ash and sulfur dioxide clouds from April 4-6, 1982, as seen with imagery from the advanced very high resolution radiometer (AVHRR) (Plates 1a, 1c, 1d, 1f, and 1h) and the total ozone mapping spectrometer (TOMS) (Plates 1b, 1e, and 1g), respectively. The mass of volcanic ash was determined using the technique of *Wen and Rose* [1994], and is shown in kg/km^2. Total column abundance of sulfur dioxide is given in Dobson units (see *Krueger et al.* [1995] for details). Note that the color scale changes to account for the decrease in sulfur dioxide and volcanic ash over time. The location of the volcano (17.33°N; 93.20°W) is indicated by the circled crosshair. (a) Composite of two AVHRR images of the volcanic ash cloud from the B eruption on April 4, 1982. The portion of the cloud east of approximately 91°W was collected at 0805 UT, and the portion to the west was collected at 0945 UT. The mass of volcanic ash cannot be determined for the opaque region of the cloud (optical depth>4), and presumably contains the greatest mass. (b) TOMS image of the sulfur dioxide cloud from the B and C eruptions on April 4, 1982 at 1820 UT. (c) AVHRR image of the volcanic ash cloud from the B and C eruptions on April 4, 1982 at 2100 UT. The mass of volcanic ash cannot be determined for the opaque region of the cloud (optical depth>4). This region is indicated by the dashed outline, and presumably contains the greatest mass. (d) Composite of two AVHRR images of the volcanic ash cloud from the B and C eruptions on April 5, 1982. The portion of the cloud east of approximately 88°W was collected at 0755 UT, and the portion to the west was collected at 0930 UT. (e) Composite of two TOMS images of the sulfur dioxide cloud on April 5, 1982. The portion of the cloud east of approximately 91°W was collected at 1700 UT, and the portion to the west was collected at 1840 UT. Three regions of high sulfur dioxide are identified (see text for discussion). (f) Composite of two AVHRR images of the volcanic ash cloud on April 5, 1982. The portion of the cloud east of approximately 107°W was collected at 2045 UT, and the portion to the west was collected at 2230 UT. (g) Composite of two TOMS images of the sulfur dioxide cloud on April 6, 1982. Three regions of high sulfur dioxide are identified (see text for discussion). The portion of the cloud east of approximately 101°W was collected at 1720 UT, and the portion to the west was collected at 1900 UT. The masses of sulfur dioxide shown for April 6 in Figure 2 includes all the cloud regions, even region 1, which is located west of the area shown. (h) Composite of two AVHRR images of the volcanic ash cloud on April 6, 1982. The portion of the cloud east of approximately 106°W was collected at 2035 UT, and the portion to the west was collected at 2215 UT. (i) Composite of two AVHRR images of the volcanic ash cloud on April 7, 1982. The portion of the cloud east of approximately 112°W was collected at 0915 UT, and the portion to the west was collected at 1050 UT.

and developed a westerly tail. A small volcanic ash cloud also extends to the south from the vent, indicating continued eruptive activity.

The last ash retrieval which we present in this paper is in shown in Plate 1i, a composite of two images collected at 0915 and 1050 UT on April 7, 1982. The main mass of ash moved south from its location in the previous scene (Plate 1h). The "tail" has become more discontinuous and continues to travel to the west. Although the volcanic cloud was visible for at least three more days in AVHRR imagery using the band difference technique, complex meteorological cloud layers under the volcanic cloud prevented the retrieval of the mass of fine volcanic ash.

6. Mass Retrievals Using TOMS and AVHRR

The results of the TOMS and AVHRR mass retrievals are shown in Figure 2 and document the injection and removal of sulfur dioxide and volcanic ash. Error bars for the TOMS sulfur dioxide retrievals are estimated at ± 30%. The AVHRR ash mass retrievals are subject to errors of at least ± 30% (see discussion, below) and reflect at least uncertainties such as determining the temperature of the surface underlying the cloud, particle size distribution assumptions, refractive index data for specific ashes, and particle shapes [*Wen and Rose*, 1994]. The timing and duration of the B and C eruptive events are indicated. Note that the first two

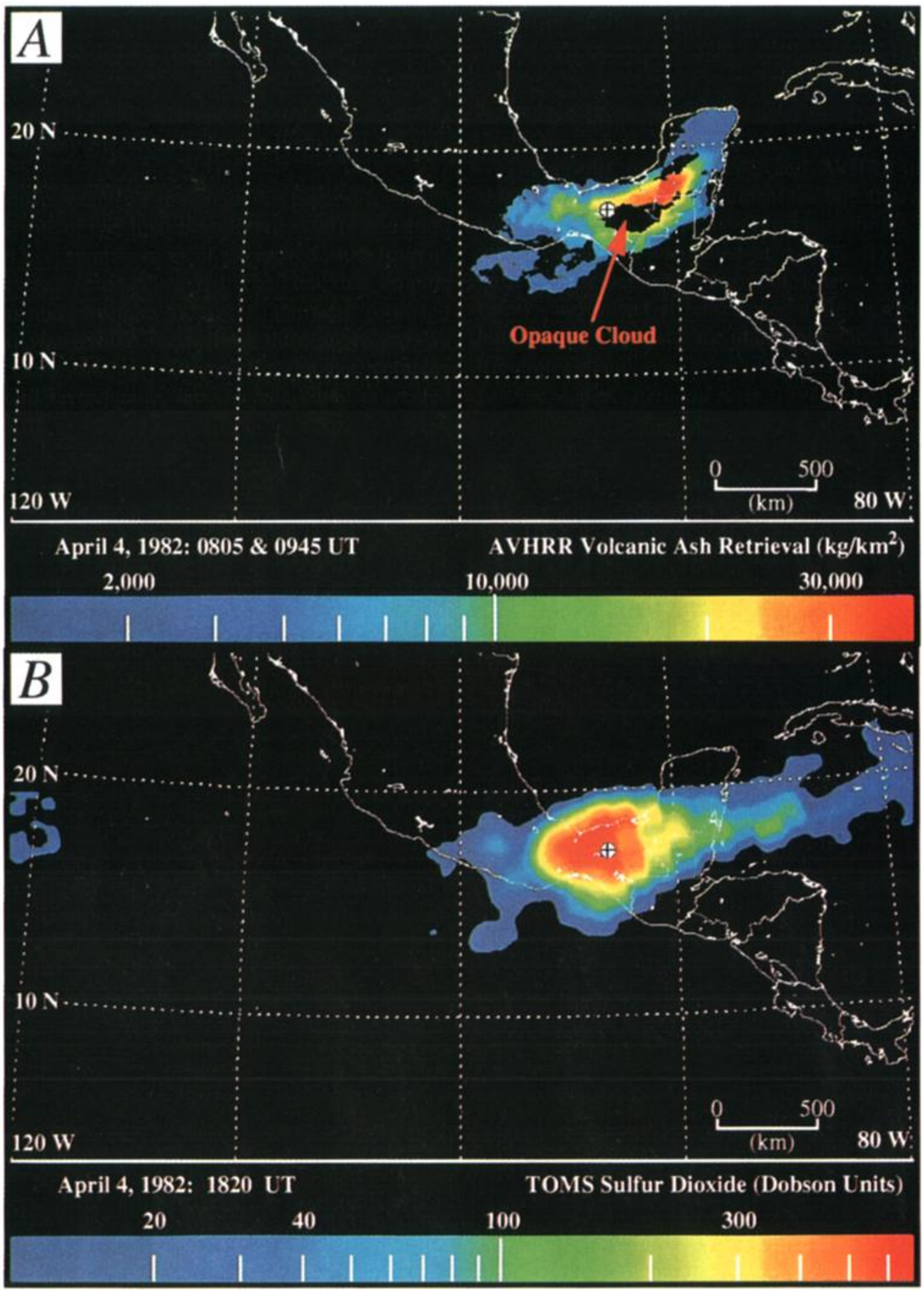

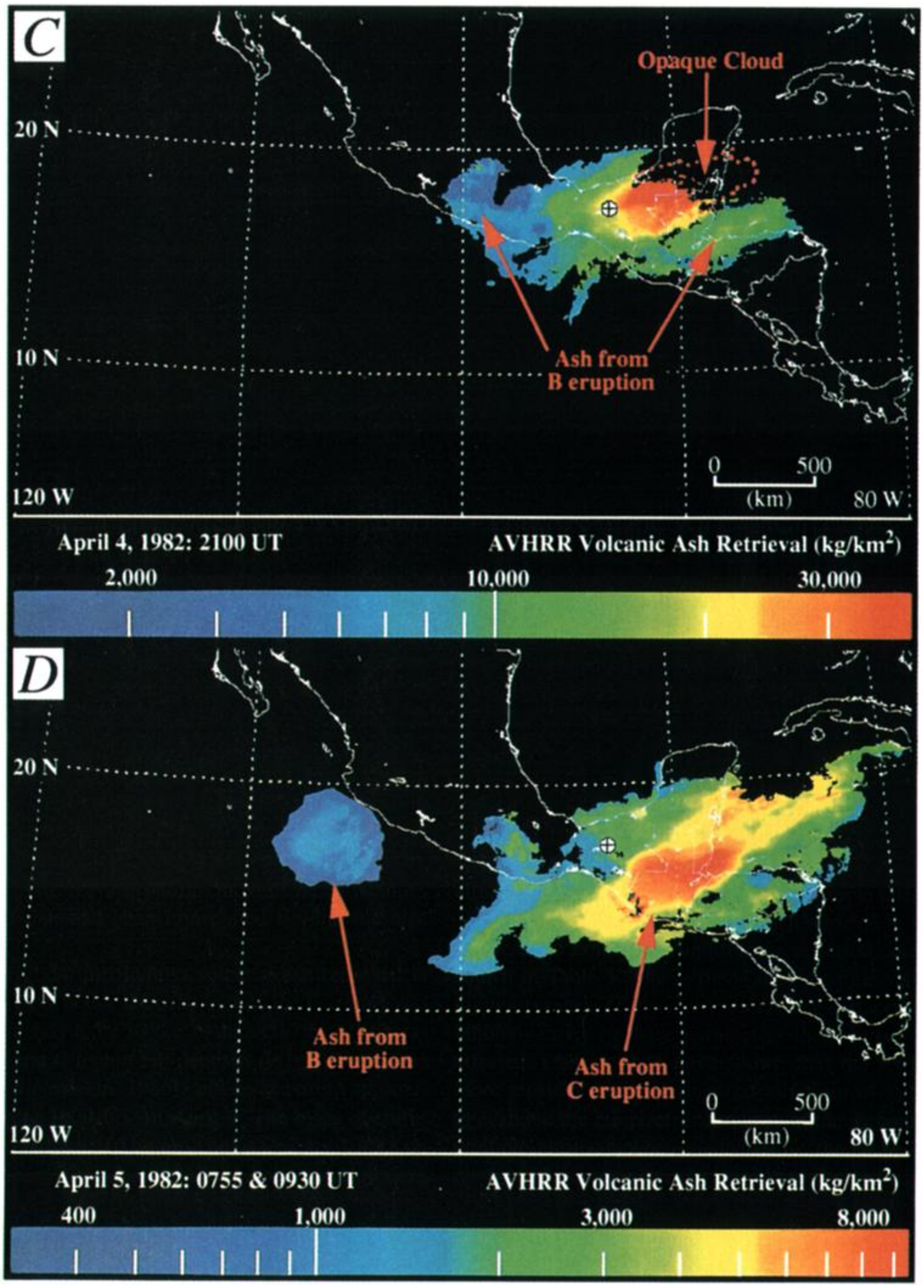

Plate 1. (continued)

ash retrievals are minimum values, because it was not possible to determine the mass of opaque regions of the volcanic clouds shown in Plates 1a and 1c. The sulfur dioxide mass includes regions of the cloud that had been transported beyond the area shown in Plate 1.

The mass of fine (1-10 μm radius) volcanic ash retrieved at 2100 UT on April 4 (2.5 hours after the end of the C event) was estimated at approximately 6.5 x 10^9 kg, or about 0.7% of the measured mass of the B and C tephra fall deposits (9.1 x 10^{11} kg, see Table 2) [*Carey and Sigurdsson*, 1986], and decreased to approximately 1.2 x 10^8 kg by 1000 UT on April 7. The mass of sulfur dioxide increased from 4.4 x 10^9 kg on April 4 to 7.1 x 10^9 kg on April 5, and was estimated at 6.8 x 10^9 kg on April 6, which is an apparent slight decrease. All three days of SO_2 mass estimates are within the absolute margin of error estimated above (± 30%), although the relative changes may be of some interest.

The sensitivity of the AVHRR ash retrieval to variability in the temperature boundary conditions was tested, and the results are shown in Table 3. The retrieval uses a single value for the cloud top temperature (T_c) and the underlying surface (T_s), so if there is inhomogeneity in these parameters the results will be adversely affected. Observations have shown that the retrievals are much more sensitive (5 to 10 times) to variations of T_s than T_c. In order to evaluate the effect of uncertainty in the T_s boundary condition, multiple retrievals were conducted for the range of values appropriate to each scene, and the results are shown in Table 3. The vari-

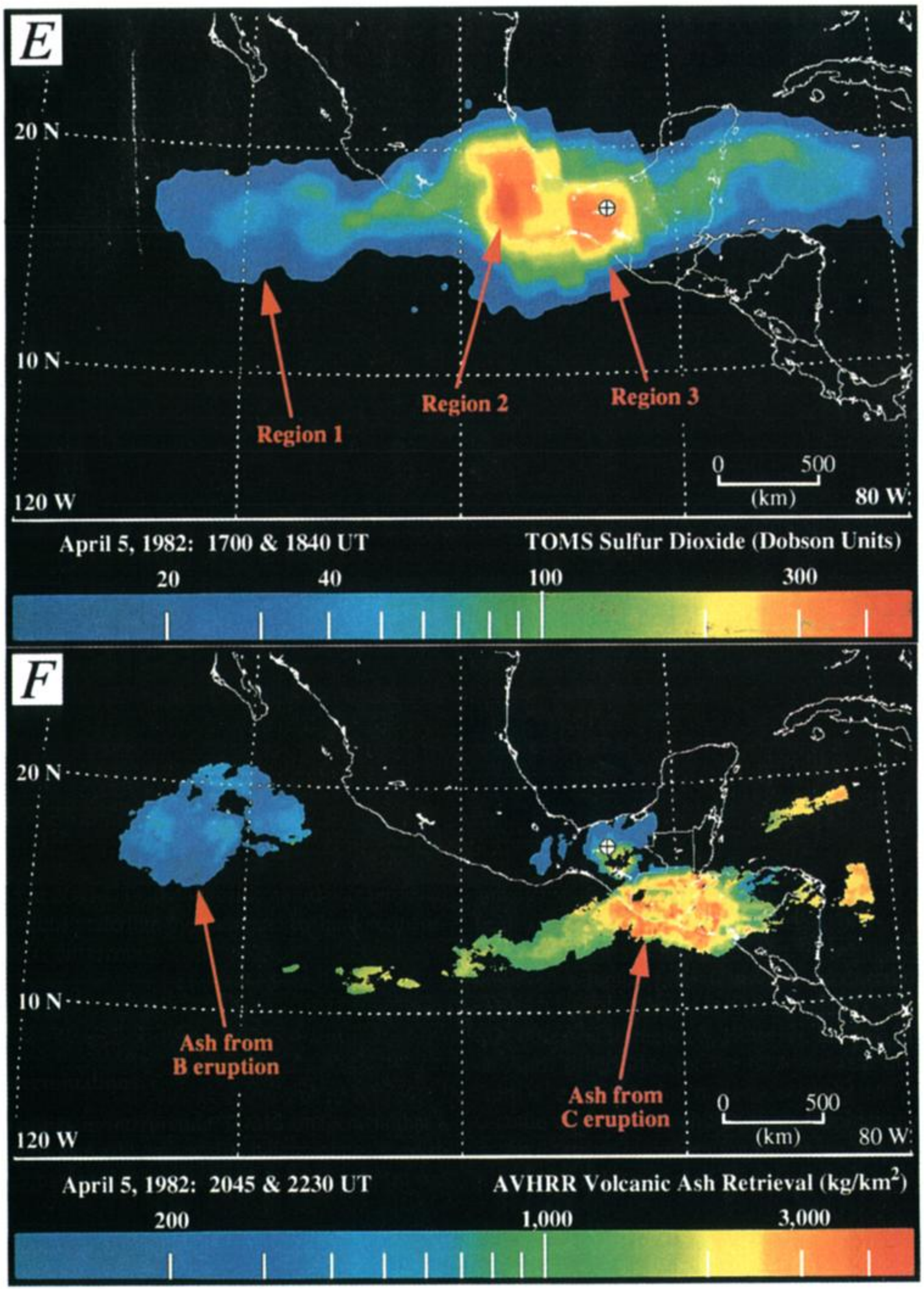

Plate 1. (continued)

ations in the retrieved mass due to an inhomogeneous background are scene specific, but generally range from 10 to 35%. The sensitivity increases as the cloud ages, and the optical depth decreases. In one case (April 5 at 2045 UT), the volcanic cloud was retrieved in two parts, the portions underlain by water and by land, to incorporate the effects of T_s differences.

7. Discussion

7.1. SO_2 Mass Determinations

One of the difficulties in interpreting TOMS imagery is that a cloud is only imaged once per day, and it is sometimes hard to relate cloud features to specific eruptive activity. Combined use of TOMS and AVHRR data allows for a more complete observation and analysis of eruptive activity than could be accomplished using a single sensor. The April 5 and 6 TOMS images (Plates 1e and 1g) show three distinct regions of high SO_2, which could not be distinguished in the image collected on April 4 (Plate 1b).

One interpretation is that the B eruption produced the SO_2 observed in region 1, the C eruption produced the SO_2 observed in region 2, and that emissions following the C eruption produced the SO_2 observed in region 3. However, the SO_2 observed in region 3 on April 5 accounts for the 60% increase in detected SO_2 from April 4 to April 5, and it seems unlikely that emissions following C could inject that much SO_2 to stratospheric heights.

An alternate interpretation is that the SO_2 observed in region 1 was emitted at the start of the B eruption, that the SO_2 observed in

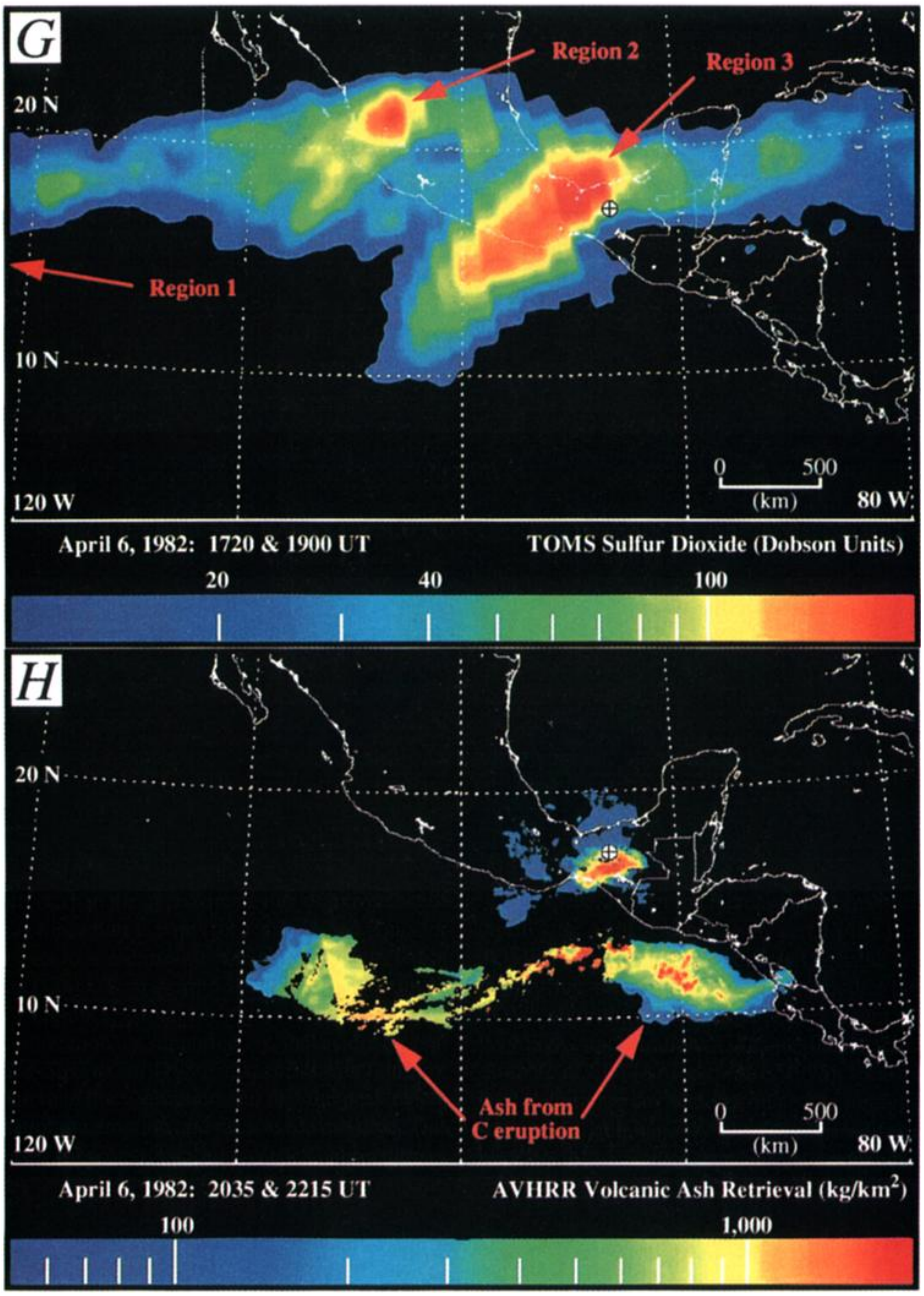

Plate 1. (continued)

region 2 was emitted during the main part of the B eruption, and that the SO_2 observed in region 3 came from the C eruption. If this interpretation is correct, then the approximate rate of movement of SO_2 would be 15 m/s for region 1, 9 m/s for region 2, and 2 m/s for region 3. Comparisons to a radiosonde wind profile collected at Veracruz, Mexico at 0000 UT on April 5 indicate an approximate height of 25 km for region 1, 23 km for region 2, and 22 km for region 3. This interpretation is supported by the evidence presented by *Carey and Sigurdsson* [1986] that the B eruption produced a higher cloud than the C eruption and that the peak height occurred at the onset of the eruption and decreased with time. This interpretation is also supported by our AVHRR observations, which show an ash cloud from the start of the B eruption (Plates 1d and 1f) following the same trajectory as the SO_2 found in region 1.

We speculate that the increase in the mass of detected SO_2 from April 4 to April 5 was due in part to the timing of the April 4 TOMS image, which was collected near the end of the C eruption but did not measure a peak mass. Another possibility is that the TOMS algorithm underestimates the amount of SO_2 in clouds with very high concentrations. Ash in volcanic clouds causes an overestimate of SO_2 [*Krueger et al.*, 1995], so ash in the cloud would tend to mitigate any underestimate due to high SO_2. *Luhr* [1990] suggested that a majority of the S released from El Chichón could have been H_2S, rather than SO_2. It seems unlikely that the mass increase was due to the emission of significant amounts of H_2S

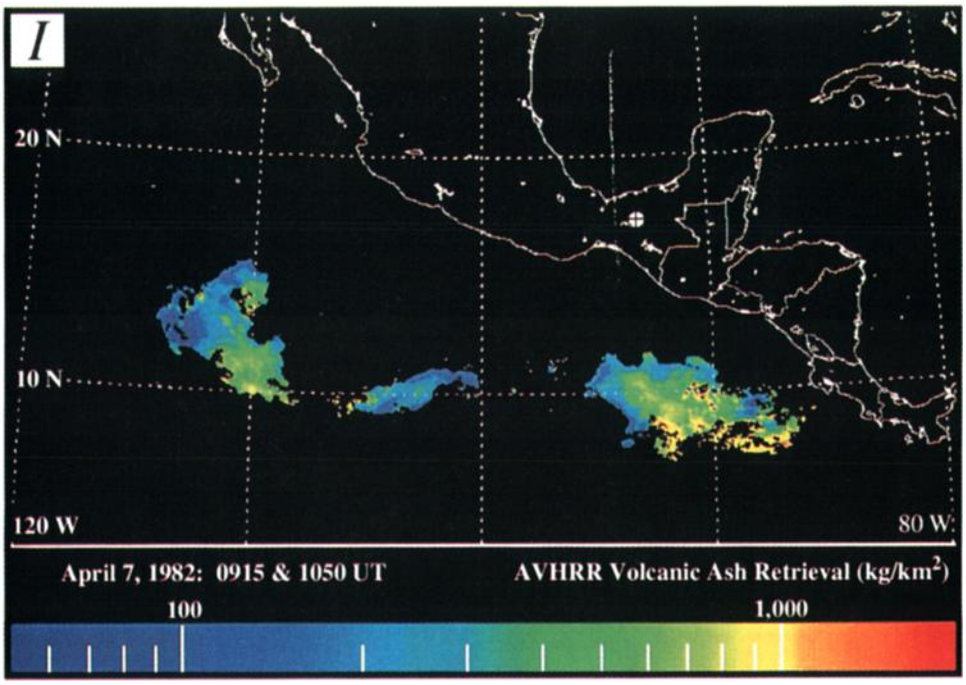

Plate 1. (continued)

Table 3. Summary of AVHRR Ash Retrievals.

Date	Time, UT	Eruption	Ts, K	Tc, K	Silicate Mass, kg	Mean Optical Depth, unitless	Mean Effective Radius, μm
April 4	0945	B	290	205	1.66×10^9	0.57	7.6
			293	205	2.20×10^9	0.63	8.0
			295	205	2.47×10^9	0.66	8.5
April 4	2100	both B and C	310	193	5.81×10^9	0.93	7.7
			315	193	6.54×10^9	1.01	8.1
			320	193	7.20×10^9	1.08	8.3
April 5	0755 and 0930	both B and C	291	193	3.13×10^9	0.37	6.8
			295	193	4.05×10^9	0.45	7.4
			298	193	4.71×10^9	0.50	7.7
April5	0930	start of B	295	226	1.91×10^8	0.14	4.8
			296	226	2.21×10^8	0.16	5.5
			297	226	2.86×10^8	0.18	6.3
April 5	2045	both B and C	land: 295 water: 294	193	total: 8.06×10^8	land: 0.27 water: 0.19	land: 4.8 water: 6.1
			land:300 water: 295	193	total: 1.10×10^9	land: 0.35 water: 0.21	land: 6.0 water: 6.4
			land: 305 water: 296	193	total: 1.42×10^9	land: 0.43 water: 0.22	land: 6.9 water: 6.6
April 5	2228	start of B	291	226	5.69×10^7	0.05	2.0
			292	226	9.55×10^7	0.07	3.1
			293	226	1.52×10^8	0.09	4.1
April5	2034 and 2214	both B and C	292	193	1.88×10^8	0.06	3.6
			293	193	2.48×10^8	0.07	4.2
			294	193	3.32×10^8	0.09	4.8
April 6	2214	start of B	283	226	1.67×10^7	0.01	1.2
			284	226	1.91×10^7	0.01	1.2
			285	226	2.22×10^7	0.01	1.3
April 7	0915 and 1050	C	east: 291 west:290	193	total: 7.46×10^7	east: 0.05 west: 0.02	east:2.7 west: 2.6
			east: 292 west: 291	193	total: 1 18 x 10^8	east: 0.06 west: 0.03	east:3.6 west: 3.8
			east: 293 west 292	193	total: 1.95×10^8	east: 0.08 west: 0.05	east: 5.0 west 5.1

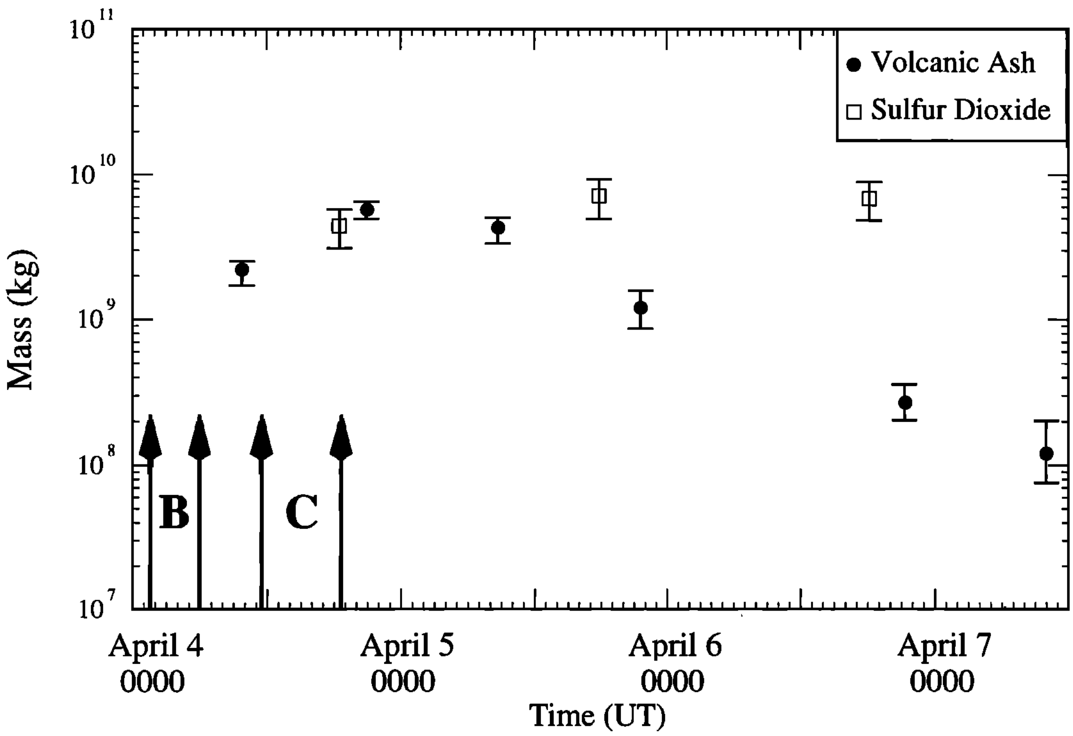

Figure 2. Mass retrievals of volcanic ash and sulfur dioxide from AVHRR and TOMS, respectively. The timing and duration of the B and C eruptive events are indicated (see text for discussion).

along with the SO_2, because the sulfur dioxide in region 3 (the youngest part of the cloud in Plate 1e) accounts for the majority of the mass increase. If a significant amount of H_2S was erupted during the B and C eruptions, one would expect the mass to increase throughout the entire cloud, unless the conversion of H_2S to SO_2 is very rapid (less than ~1 hour 1/*e*). Based on *Graedel* [1977], H_2S is thought to have a lifetime of about 1 day in the troposphere and converts to SO_2.

We speculate that the hypothesis applied to Pinatubo involving a separate vapor phase of SO_2 [*Gerlach et al.*, 1996] could be a factor in enhancing separation of El Chichón eruptions B and C, because the ash-poor, SO_2-rich phase might escape first and perhaps rise higher in the early part of each eruption. We have no way to prove such a process with our data, but our data are consistent with it.

7.2. Retrievals of mass of fine ash using AVHRR

The ash detection method used here differs from the one employed by *Robock and Matson* [1983] even though both are based on data from weather satellites. They looked at scattering of the visible wavelengths and most likely detected smaller (<1 μm) particles, perhaps including sulfate aerosols, while the thermal infrared band subtraction method we employ is most sensitive to ash and sulfate particles between 1 and 10 μm in radius. Although, theoretically, the technique we employ cannot uniquely distinguish silicate ash from sulfate aerosol [*Prata*, 1989; *Wen and Rose*, 1994], there is strong evidence that the cloud detected by the AVHRR was composed primarily of ash.

We considered what type of sulfate particles could produce the observed AVHRR signal if no silicate ash particles were present in the volcanic cloud. A model volcanic cloud retrieval, using the refractive index for a 75% H_2SO_4 / 25% H_2O aerosol (rather than andesite), gives a particle mean effective radius of 1.75 μm for the cloud imaged by the AVHRR on April 4 (Plate 1c), a value which is 1-2 orders of magnitude too large. *Hofmann and Rosen* [1983] sampled the cloud at 24.5-25.5 km, 45 days after the eruption, and found that the sulfate aerosol had a bimodal particle distribution. The smaller particles (mode radius near 0.02 μm) consisted of newly nucleated sulfate droplets, and the larger particles (mode radius near 0.70 μm) were believed to have been formed by the growth of the preeruption aerosol due to the accretion of sulfuric acid vapor. In addition, model results by *Turco et al.* [1983] show that "pure" sulfate aerosols can only grow to a size of about 0.02-0.20 μm. Comprehensive study of the 1991 Pinatubo aerosol [*Russell et al.*, 1996] shows that 65-80% H_2SO_4 was the composition of most Pinatubo sulfates and that their effective radii were generally 0.1- 0.2 μm during the first month and grew to as large as 0.5- 0.6 μm after several months, reflecting coagulation processes. However, even if the El Chichón cloud was composed of sulfate particles with a radius of 1.75 μm, the settling velocity of particles of that size is too low for them to have fallen far enough to produce the observed separation. In addition, analysis of TOMS reflectivity data by *Seftor et al.* [1997] detected a volcanic ash cloud in the same location as the cloud detected by the AVHRR. They used a two-channel reflectivity difference (340 - 380 nm) to distinguish absorbing particles, such as volcanic ash, desert dust, and smoke, from nonabsorbing particles, such as sulfate aerosol and meteorological clouds. Thus it is likely that the signal measured by the AVHRR is dominated by silicate ash, and not sulfate.

The mass estimates computed with two-band IR data from AVHRR give information about the sizes, optical depths, and masses of particles that scatter within the Mie range of 10-12 μm electromagnetic energy. This means that the retrieval model is

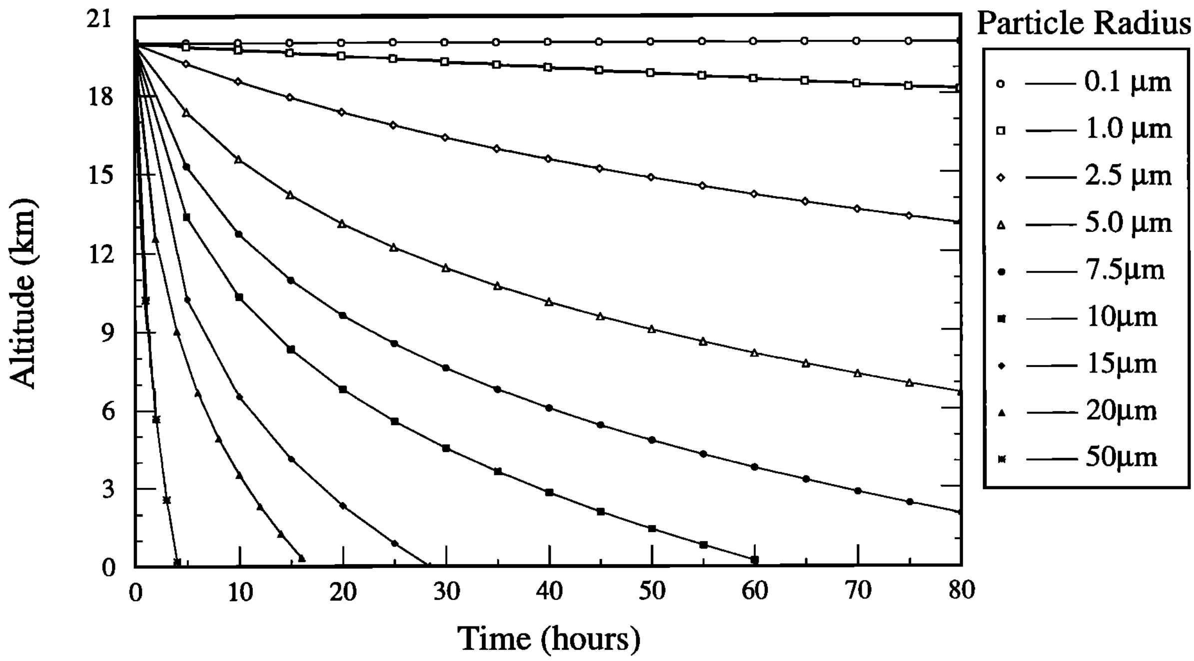

Figure 3. Fall distances for spherical, 0.1-50 µm radius, volcanic ash particles as a function of time. The local viscosity was determined from a radiosonde temperature profile collected at Veracruz, Mexico (380 km NW of El Chichón) on April 5 at 0000 UT.

only sensitive to particles with radii between about 1 and 10 µm, and the mass retrieved is only a part of the total particle mass in the cloud.

Large (>50 µm) particles are the largest (>95%) fraction of the total mass of erupted silicates in eruptions, but these particles fall out very quickly (<5 hours) and none of these is sensed by AVHRR. In order to demonstrate the effects of particle settling on the retrieved mass of volcanic ash, fall times were computed using Stokes' law for a range (0.1-50 µm) of particle radii, and the results are shown in Figure 3. The gravitational settling velocity of ash particles in a laminar regime (low Reynolds number) is governed by the particle density, size, shape, and local viscosity of the medium (air) [*Fuchs*, 1989]. We assume the ash to be spherical particles having a specific gravity of 2.6 (dense trachyandesite) and an initial cloud height of 20 km. The local viscosity was determined from a radiosonde temperature profile collected at Veracruz, Mexico (380 km NW of El Chichón) on April 5 at 0000 UT. Actual ash particles may fall more slowly than these calculations indicate, due to turbulence, and increased drag as a result of their nonspherical shape. *Mackinnon et al.* [1984] calculated fall rates for nonspherical particles using Wilson-Huang equations [*Wilson and Huang*, 1979] and found that the terminal velocity was a factor of 2 slower than for spheres, and thus these calculations presented here may represent maximum fall rates. Particles between 10 and 50 µm radius are not sensed by AVHRR, but Figure 3 suggests that a significant fraction of particles in this size range would be expected to remain in the ash cloud up to tens of hours after the eruptions and go undetected. It is one of the challenges of volcanic remote sensing to figure out a way to detect particles in this size range. The fast fallout rate of large particles is nevertheless likely to be the main explanation for the observation that the retrieved fine particle masses (1-10 µm radii) in the El Chichón clouds are only slightly less than 1% of the mass measured in the fall deposit. It is also possible that there is a missing (undetected by AVHRR) mass of larger silicate particles (perhaps aggregates as the works of *Sorem* [1982] and *Mackinnon et al.* [1984] suggest) in the El Chichón clouds.

We find the gravitational settling of small particles under 1 µm to be negligible (under 20 m) over the duration of interest (2-3 days). However, the settling is significant for ash particles with radii in the 1-10 µm radius range, the size range that can be detected and retrieved using AVHRR. The greatest decrease in detected mass occurred between the images shown in Plates 1d and 1f, and we speculate that fallout is an important factor in the mass decrease, rather than just dispersion of the cloud until it was no longer detected. The ash cloud shown in Plate 1d, is being sheared at the top, to the SW, by stratospheric winds, and at the bottom, to the NE, by tropospheric winds. However, the ash cloud shown in Plate 1f, is only being sheared at the top, indicating that masses of ash at lower levels had decreased considerably. Subsequent observations only show shear to the west. Our contention that fallout is a dominant factor in the observed mass decrease is supported by a decrease in the retrieved particle size over time (Figure 4), which reflects the removal of a coarser size fraction. We speculate that precipitation from the tropospheric volcanic cloud may have been occurring, accelerating particle fallout. Dispersion of the cloud beyond the limit of detection is likely to be a progressively more important factor in the mass trend as the thinning cloud ages, however.

The retrieved mass from AVHRR data is not a good way to estimate the total amounts of missing distal fallout as discussed by many volcanologists [*Rose*, 1993; *Bonadonna et al.*, 1998]. There are at least three reasons for this: First, there are limitations in sizes or particles sensed, as discussed above. Second, particles may aggregate and not behave as isolated scatterers in volcanic clouds [*Sorem*, 1982; *Carey and Sigurdsson*, 1982; *Gilbert and Lane*, 1994]. Third, simplifying assumptions of the retrieval model are not achieved in a real situation: (1) spherical shapes for cloud

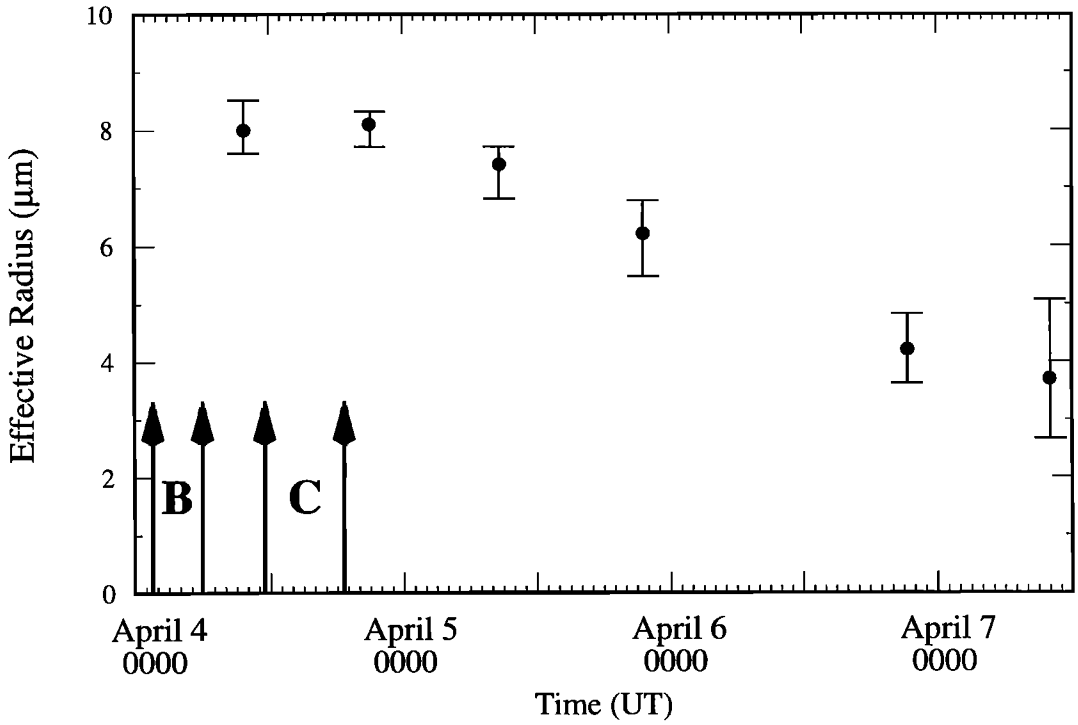

Figure 4. Mean effective radius of the volcanic ash from the El Chichón clouds, as a function of time. Error bars indicate uncertainty in the surface temperature boundary condition. The timing and duration of the B and C eruptions are indicated (see text for discussion).

particles, (2) a single cloud layer, (3) a simple background for the cloud with a uniform higher temperature, (4 a cloud that is semi-transparent, (5) a lognormal particle size distribution with a sorting that resembles ash fallout, and (6) a clear atmosphere above or, in fact, below the volcanic cloud. We know that many of these assumptions are not valid: (1) ash particles are not spherical, (2) many volcanic clouds are not single layers, (3) backgrounds are frequently very complex, consisting of clouds and land or water at various heights and temperatures, (4) clouds are sometimes opaque (e.g., Plate 1a), and (5) the lognormal assumption is not well supported by volcanic cloud particle sampling data. *Carey and Sigurdsson* [1986], using estimates of eruption rates based on heights of columns and area thickness data extrapolations, estimated that more than half of the total volume of El Chichón fallout deposit was deposited outside of the last measured isopach map contour. Because of the uncertainties about the quantitative mass retrievals, we hesitate to emphasize the significance of the low mass proportion of fine ash retrieved in El Chichón clouds (0.7%). Instead, we think retrieval results are more meaningful in a relative sense (compared to each other) where they demonstrate rapid decline of masses, optical depths, and particle sizes with time over a 3- day period.

The mass retrievals demonstrate dramatic differences in the residence times of volcanic ash and sulfur dioxide in the atmosphere (Figure 2). Following the increase in the mass of detected SO_2 from April 4 to April 5, the TOMS retrievals show a 4% decrease in the mass from April 5 to April 6. Although the decrease is small compared to the errors of measurement, a slow decreasing trend for SO_2 mass is typical of volcanic clouds emplaced in the stratosphere [*Bluth et al.*, 1992], and increases 1 day after eruptive events have also been noted in the cases of all three 1992 Spurr events [*Bluth et al.*, 1995] and for the May 18, 1980, Mount St. Helens eruption [*Bluth et al.*, 1997]. In contrast to TOMS, the AVHRR retrievals show a rapid decrease in the mass of detected ash following the eruption. It decreased by 25% in the 15 hours after the end of the C eruption, and by 98% in 64 hours. In general, the mass of SO_2 detected by TOMS decreases as a function of time due to the chemical conversion of SO_2 to sulfate, and the mass of volcanic ash decreases due to the fallout of ash particles, perhaps aided by meteorological precipitation. In addition, the mass of each constituent can decrease due to physical dispersion of the cloud at its edge to levels beneath the detection limit. An important factor in the rapid relative decline of particle mass is the fact that silicate ash was mainly tropospherically dispersed, while SO_2 was emplaced in the stratosphere.

7.3. Separation of the El Chichón Clouds

We interpret the observations of separation described above to be the result of the vertical segregation of SO_2 and volcanic ash, possibly due to gravitational processes. *Holasek et al.* [1996] showed experimentally that sedimentation of ash particles in plumes can produce vertical separation of gas-rich and particle-rich portions. In their experiments, the gas-rich portion of the plume ascended and the denser, particle-rich portion descended until it reached its neutral buoyancy height. The presence of the strong wind shear during and following the eruption of El Chichón resulted in very different trajectories for sulfur dioxide and volcanic ash. Our observations show that the principal mass of SO_2 moved to the west of the vent at heights of approximately 22-26 km, and the principal mass of ash moved to the east and south of the vent at heights of about 19-21 km.

Separation of SO_2 and ash is important for the mitigation of aircraft hazards, and it also is potentially important in understanding the reactions that occur in volcanic clouds. The TOMS instrument

may be used for tracking volcanic clouds which are hazardous to aircraft, but this needs to be done with caution, because it is volcanic ash which poses the greatest hazard to aircraft engines [*Casadevall,* 1994]. The presence of volcanic ash probably affects the conversion rate of SO_2 to sulfate and provides a substrate for chemical reactions [*Turco et al.,* 1983]. Separation of the gas and the ash could slow the rate of conversion of SO_2 into sulfate aerosol and may tend to decrease the scavenging of volcanic aerosol by ash [*Rose,* 1977; *Tabazadeh and Turco,* 1993]. We note that the radiative transfer model used to determine the amount of SO_2 from the TOMS data does not account for the presence of ash. *Krueger et al.* [1995] reported that the ash in volcanic clouds will result in overestimation of SO_2, so separation must affect the TOMS SO_2 calculations.

Evidence for separation of ash and gas in several volcanic clouds of Galunggung was noted by *Bluth et al.* [1994], and we speculate that it may be common in many eruptions. The presence of a strong wind shear is a primary factor in determining whether the separation will be observed in satellite images. Although a comparison between TOMS and AVHRR of clouds from and the August 1992 eruption of Mount Spurr [*Krotkov et al.,* in press] showed that the gas and ash followed similar trajectories, these clouds were transported mainly in the upper troposphere. Separation is most likely observed if the maximum height of an eruption column reaches a level a few kilometers above the level of the wind shear. For the El Chichón example, the ash from the start of the B eruption was too high for early separation to be observed because the sedimentation in the column occurred in the stable, unsheared stratosphere. However, the majority of the ash from the latter part of B and from the C eruptions only reached a height near, or a few kilometers above, the tropopause. Subsequent sedimentation of the ash through a significant shear allowed for a striking separation to be observed.

The TOMS and AVHRR observations described above provide new insights into the balloon-borne sampling of the El Chichón aerosol conducted by *Hofmann and Rosen* [1983] in the months following the eruption. They found two distinct sulfate aerosol layers, centered at 25 km and 18 km, separated by a clean region, a nonvolatile layer (presumably ash) at approximately 16 km. Moreover they report that the layer at 25 km was more sulfur-rich (~ 80% H_2SO_4 solution) than the layer at 18 km (~ 60-65% H_2SO_4 solution). They proposed that the higher layer may have been produced by the C eruption, while the layers at 18 km and 16 km may have been produced by the A-1 and (or) the B eruption(s). Although the observations presented in this paper support the hypothesis of Hofmann and Rosen that the aerosol layers were produced by two different eruptions, we believe that the majority of SO_2 from both the B and C eruptions was emplaced at 22-23 km, and that ash from both of these events produced the nonvolatile layer observed at 16 km. We note also that the 1980 Mount St. Helens eruption column was stratospheric in height, but most of its dispersal was in the troposphere [*Holasek and Self,* 1995; *Woods et al.,* 1995].

8. Conclusions

This paper demonstrates the utility of using multiple satellite sensors to analyze explosive volcanic activity. Until recently, very few direct comparisons have been made between TOMS and AVHRR. However, there is a 15 year archive of data, and a large potential for future work. The comparisons presented in this paper document the separation of sulfur dioxide and volcanic ash in the atmosphere, possibly due to the vertical segregation of the volcanic cloud constituents by gravitational processes. A theory of gravitational separation has been developed from experimental evidence [*Holasek et al.,* 1996], but never before evaluated with satellite imagery. The presence of a strong wind shear is a primary factor in determining whether the separation will be observed in satellite imagery. Separation is most likely observed if the maximum height of an eruption column reaches a level a few kilometers above the level of the wind shear. Mass retrievals of sulfur dioxide and ash highlight the difference in residence times of these constituents in the atmosphere. Mostly in the troposphere, the mass of fine (1-10 μm) volcanic ash decreased by 98% in 64 hours, while the mass of sulfur dioxide in the stratosphere declined much more slowly. More work needs to be done to determine how representative the El Chichón results are of the fate of volcanic ash in the atmosphere. The separation of ash and SO_2 is important to the study of atmospheric reactions and the mitigation of volcanic hazards.

Acknowledgments. This work was completed while DJS was supported as a NASA Global Change Fellow. Research funding came from NASA and NSF. The paper benefited from reviews by Stephen Self and Gerald Ernst.

References

Bluth, G. J. S., S. D. Doiron, C. C. Schnetzler, A. J. Krueger, and L. S. Walter, Global tracking of the SO_2 clouds from the June, 1991 Mount Pinatubo eruptions, *Geophys. Res. Lett., 19,* 151-154, 1992.

Bluth, G. J. S., T. J. Casadevall, C. C. Schnetzler, S. D. Doiron, L. S. Walter, A. J. Krueger, and M. Badruddin, Evaluation of sulfur dioxide emissions from explosive volcanism: The 1982-1983 eruptions of Galunggung, Java, Indonesia, *J. Volcanol. Geotherm. Res., 63,* 243-256, 1994.

Bluth, G. J. S., C. J. Scott, I. E. Sprod, C. C. Schnetzler, A. J. Krueger, and L. S. Walter, Explosive emissions of sulfur dioxide from the 1992 Crater Peak eruptions, Mount Spurr volcano, Alaska, in *The 1992 Eruptions of Crater Peak Vent, Mount Spurr Volcano, Alaska,* edited by T. E. C. Keith, pp. 37-45, *U.S. Geol. Surv. Bull., 2139,* 1995.

Bluth, G. J. S., W. I. Rose, I. E. Sprod, and A. J. Krueger, Stratospheric loading of sulfur from explosive volcanic eruptions, *Geology, 105,* 671-683, 1997.

Bonadonna, C., G. G. J. Ernst, and R.S.J. Sparks, Thickness variations and volume estimates of tephra fall deposits: The importance of particle Reynolds number, *J. Volcanol. Geotherm. Res., 81,* 173-188, 1998.

Carey, S., and H. Sigurdsson, Influence of particle aggregation on deposition of distal tephra from the May 18, 1980 eruption of Mount St. Helens volcano, *J. Geophys. Res., 87,* 7061-7072, 1982.

Carey, S., and H. Sigurdsson, The 1982 eruptions of El Chichón volcano, Mexico, 2, Observations and numerical modeling of tephra-fall distribution, *Bull. Volcanol., 48,* 127-141, 1986.

Casadevall, T. J. (Ed.), Volcanic Ash and Aviation Safety: Proceedings of the First International Symposium on Volcanic Ash and Aviation Safety, *U.S. Geol. Surv. Bull., 2047,* 450 pp., 1994.

DeLuisi, J. J., E. G. Dutton, K. L. Coulson, T. E. DeFoor, and B. E. Mendonca, On some radiative features of the El Chichón volcanic stratospheric dust cloud and a cloud of unknown origin observed at Mauna Loa, *J. Geophys. Res., 88,* 6769-6772, 1983.

Fuchs, N. A., *The Mechanics of Aerosols,* Dover, New York, 408 pp.,1989.

Gerlach, T. M., H. R. Westrich, and R. B. Symonds, Preeruption vapor in magma of the climactic Mount Pinatubo eruption: Source of the giant stratospheric sulfur dioxide cloud, in *Fire and Mud Eruptions and lahars of Mount Pinatubo, Philippines,* edited by C. G. Newhall and R. S. Punongbayan, pp. 415-434, Univ. of Wash. Press, Seattle, 1996.

Gilbert, J. S., and S. J. Lane, The origin of accretionary lapilli, *Bull. Volcanol., 56,* 398-411, 1994.

Graedel, T. E., The homogeneous chemistry of atmospheric sulfur, *Rev. Geophys., 15,* 421-428, 1977.

Hofmann, D., and J. M. Rosen, Stratospheric sulfuric acid fraction and mass estimate for the 1982 volcanic eruption of El Chichón, *Geophys. Res. Lett., 10,* 313-315, 1983.

Holasek, R. E., and S. Self, GOES weather satellite observations and measurements of the May 18, 1980 Mount St. Helens eruption, *J. Geophys. Res., 100*, 8469-8487, 1995.

Holasek, R. E., A. W. Woods, and S. Self, Experiments on gas-ash separation processes in volcanic umbrella plumes, *J. Volcanol. Geotherm. Res., 70*, 169-181, 1996.

Krotkov, N. A., A. J. Krueger, and P. K. Bhartia, Ultraviolet optical model of volcanic clouds for remote sensing of ash and sulfur dioxide, *J. Geophys. Res., 102*, 21891-21904, 1997.

Krotkov, N. A., O. Torres, C. Seftor, A. J. Krueger, W. I. Rose, A. Kostinski, G. J. S. Bluth, D. J. Schneider and S. J. Schaefer, Comparison of TOMS and AVHRR volcanic ash retrievals from the August 1992 eruptions of Mount Spurr, *Geophys. Res. Lett.*, in press.

Krueger, A. J., L. S. Walter, P. K. Bhartia, C. C. Schnetzler, N. A. Krotkov, I. Sprod, and G. J. S. Bluth, Volcanic sulfur dioxide measurements from the total ozone mapping spectrometer instruments, *J. Geophys. Res., 100*, 14057-14076, 1995.

Luhr, J.F., Experimental phase relations of water- and sulfur-saturated arc magmas and the 1982 eruptions of El Chichón volcano, *J. Petrol., 31*, 1071-1114, 1990.

Mackinnon, I. D., R., J. L. Gooding, D. S. McKay, and U. S. Clanton, The El Chichón stratospheric cloud: Solid particulates and settling rates, *J. Volcanol. Geotherm. Res., 23*, 125-146, 1984.

Matson, M., The 1982 El Chichón volcano eruptions - A satellite perspective, *J. Volcanol. Geotherm. Res., 23*, 1-10, 1984.

McCormick, M. P., T. J. Swissler, W. H. Fuller, W. H. Hunt, and M. T. Osborn, Airborne and ground-based lidar measurements of the El Chichón aerosol from 90°N to 56°S, *Geofis. Int., 23*, 187-221, 1984.

McCormick, M. P., L. W. Thomason, and C. R. Trepte, Atmospheric effects of the Mt. Pinatubo eruption, *Nature, 373*, 399-404, 1994.

McPeters, R., P. K. Bhartia, A. J. Krueger, J. R. Herman, B. M. Schlesinger, G. G. Wellemeyer, C. J. Seftor, G. Jaross, S. L. Taylor T. Swissler, O. Torres, G. Labow, W. Byeyly, and R. P. Cebula, Nimbus-7 total ozone mapping spectrometer (TOMS) data products users guide, *NASA Ref. Publ., RP-1384*, 67pp., 1996.

Pinto, J. P., R. P. Turco, and O. B. Toon, Self-limiting physical and chemical effects in volcanic eruption clouds, *J. Geophys. Res., 94*, 11165-11174, 1989.

Prata, A. J., Infrared radiative transfer calculations for volcanic ash clouds, *Geophys. Res. Lett., 16*, 1293-1296, 1989.

Robock, A., and M. Matson, Circumglobal transport of the El Chichón volcanic dust cloud, *Science, 221*, 195-197, 1983.

Rose, W. I., Scavenging of volcanic aerosol by ash: Atmospheric and volcanologic implications, *Geology, 5*, 621-624, 1977.

Rose, W. I., Comment on "Another look at the calculation of fallout tephra volumes" by Judy Fierstein and Manuel Nathenson, *Bull. Volcanol., 55*, 372-374, 1993.

Rose, W. I., and C. A. Chesner, Dispersal of ash in the great Toba eruption, 75 ka, *Geology, 16*, 913-917, 1987.

Rose, W. I., and D. J. Schneider, Satellite images offer aircraft protection from volcanic ash clouds, *Eos Trans. AGU, 77*, 529-532, 1996.

Rose, W. I., D. J. Delene, D. J. Schneider, G. J. S. Bluth, A. J. Krueger, I. Sprod, C. McKee, H. L. Davies, and G. G. J. Ernst, Ice in the 1994 Rabaul eruption cloud: Implications for volcanic hazard and atmospheric effects, *Nature, 375*, 477-479, 1995.

Russell, P. B., J. M. Livingston, R. F. Pueschel, J. J. Bauman, J. B. Pollack, S. L. Brooks, P. Hamill, L. W. Thomason, L. L. Stowe, T. Deshler, E. G. Dutton, and R. W. Bergstrom, Global to microscale evolution of the Pinatubo volcanic aerosol derived from diverse measurements and analyses, *J. Geophys. Res., 101*, 18745-18763, 1996.

Schneider, D. J., W. I. Rose, and L. Kelley, Tracking of 1992 eruption clouds from Crater Peak vent of Mount Spurr volcano, Alaska, using AVHRR, in *The 1992 Eruptions of Crater Peak Vent, Mount Spurr Volcano, Alaska*, edited by T. E. C. Keith, pp. 27-36, *U.S. Geol. Surv. Bull., 2139*, 1995.

Schoeberl, M. R., L. R. Lait, P. A. Newman, and J. E. Rosenfield, The structure of the polar vortex, *J. Geophys. Res., 97*, 7859-7882, 1992.

Seftor, C. J., N. C. Hsu, J. R. Herman, P. K. Bhartia, O. Torres, W. I. Rose, D. J. Schneider, and N. Krotkov, Detection of volcanic ash clouds from Nimbus-7/TOMS reflectivity data, *J. Geophys. Res., 102*, 16749-16760, 1997.

Self, S., M. R. Rampino, and J. J. Barbera, The possible effects of large 19th and 20th century volcanic eruptions on zonal and hemispheric surface temperatures, *J. Volcanol. Geotherm. Res., 11*, 41-60, 1981.

Sigurdsson, H., S. N. Carey, and J. M. Espindola, The 1982 eruptions of El Chichón volcano, Mexico: Stratigraphy of pyroclastic deposits, *J. Volcanol. Geotherm. Res., 23*, 11-37, 1984.

Sorem, R. K., Volcanic ash clusters: Tephra rafts and scavengers, *J. Volcanol. Geotherm. Res., 13*, 63-71, 1982.

Tabazadeh, A., and R. P. Turco, Stratospheric chlorine injection by volcanic eruptions: HCl scavenging and implications for ozone, *Science, 260*, 1082-1086, 1993.

Turco, R. P., O. B. Toon, R. C. Whitten, P. Hamill, and R. G. Keesee, The 1980 eruptions of Mount St. Helens: Physical and chemical processes in the stratospheric clouds, *J. Geophys. Res., 88*, 5299-5319, 1983.

Varekamp, J. C., J. F. Luhr, and K. L. Prestegaard, The 1982 eruptions of El Chichón volcano (Chiapas, Mexico): Character of the eruptions, ash-fall deposits, and gas phase, *J. Volcanol. Geotherm. Res., 23*, 39-68, 1984.

Wen S., and W. I. Rose, Retrieval of sizes and total masses of particles in volcanic clouds using AVHRR bands 4 and 5, *J. Geophys. Res., 99*, 5421-5431, 1994.

Wilson, L., and T. C. Huang, The influence of shape on the atmospheric settling of volcanic ash particles, *Earth Planet. Sci. Lett., 44*, 311-324, 1979.

Woods, A. W., R. E. Holasek, and S. Self, Wind-driven dispersal of volcanic ash plumes and its control on the thermal structure of the plume top, *Bull. Volcanol., 57*, 283-292, 1995.

Yamanouchi, T., K. Suzuki, and S. Kawaguchi, Detection of clouds in Antarctica from infrared multispectral data of AVHRR, *J. Meteorol. Soc. Jpn., 65*, 949-961, 1987.

G. J. S. Bluth, L. R. Coke, and W. I. Rose, Department of Geological Engineering and Sciences, Michigan Technological University, Houghton, MI 49931. (email: gbluth@mtu.edu; lrcoke@mtu.edu; raman@mtu.edu)

A. J. Krueger, Code 916, Goddard Space Flight Center, Greenbelt, MD 20771. (email: krueger@chapman.gsfc.nasa.gov)

D. J. Schneider, Alaska Volcano Observatory, 4200 University Drive, Anchorage, AK, 99508. (email: djschneider@usgs.gov)

I. E. Sprod, Cooperative Institute for Research in Environmental Sciences, Campus Box 216, Boulder, CO 80309-0216. (email: ian@ngdc.noaa.gov)

(Received May 12, 1998; revised October 21, 1998; accepted October 27, 1998.)